THE ASTROPHYSICAL JOURNAL, 465:L133–L136, 1996 July 10

A SIMPLE MODEL OF SPECTRAL-LINE PROFILES FROM CONTRACTING CLOUDS

P. C. MYERS, D. MARDONES, M. TAFALLA, J. P. WILLIAMS, AND D. J. WILNER
Harvard-Smithsonian Center for Astrophysics, 60 Garden Street, Cambridge MA 02138; pmyers, dmardones, mtafalla, jpw, dwilner@cfa.harvard.edu
Received 1996 March 11; accepted 1996 April 25

ABSTRACT

A simple analytic model of radiative transfer in two parts of a contracting cloud matches a wide range of line profiles in candidate infall regions and provides a sensitive estimate of V_{in}, the characteristic inward speed of the gas forming the line. The model assumes two uniform regions of equal temperature and velocity dispersion σ, whose density and velocity are attenuation-weighted means over the front and rear halves of a centrally condensed, contracting cloud. The model predicts two-peak profiles for "slow" infall, $V_{in} \ll \sigma$, and red-shoulder profiles for "fast" infall, $V_{in} \sim \sigma$. A simple formula expresses V_{in} solely in terms of σ and of observable parameters of a two-peak line. We apply the model to fit profiles of high and low optical depth lines observed in a dense core with no star (L1544, $V_{in} = 0.006$ km s^{-1}), with an isolated protostar (L1527, 0.025 km s^{-1}), and with a small group of stars (L1251B, 0.35 km s^{-1}). The mass infall rate obtained from V_{in} and the map size varies from (2–40) $\times 10^{-6}$ $M_\odot$ yr^{-1} and agrees within a factor $\sim$2 in each core with the independently determined rate $\sim\sigma^3\ G^{-1}$ for a gravitationally collapsing isothermal sphere. This agreement suggests that the inward motions derived from the line profiles are gravitational in origin.

Subject headings: ISM: molecules — line: profiles — stars: formation

1. INTRODUCTION

Recent advances in the performance of millimeter-wavelength telescopes have begun to yield kinematic evidence of gravitational motions associated with the formation of stars. Studies based on multiple line maps have led to plausible claims of inward motions in regions forming low-mass stars, including B335 (Zhou et al. 1993, 1994) and L1527 (Mardones et al. 1994; Zhou et al. 1994; Myers et al. 1995). Spectral-line surveys of very red sources have begun to reveal new infall candidates (Wang et al. 1995; Gregerson et al. 1996; Mardones et al. 1996).

The line profiles in candidate infall sources have been interpreted with detailed numerical models (e.g., Leung & Brown 1977; Leung 1978; Bernes 1979; Walker et al. 1986; Walker, Narayanan, & Boss 1994). Agreement between these models and observed line profiles of CS and H_2CO (Zhou et al. 1993; Myers et al. 1995; Choi et al. 1995) is encouraging, and has determined the infall radius of B335 and L1527 to be 0.02–0.04 pc in the inside-out collapse theory of Shu (1977). But fitting such complex models is slow and laborious. This difficulty limits efforts to determine whether the many profiles observed in surveys and maps of infall candidates are generally consistent with gravitational infall. A simple infall model is needed to extract more easily the kinematic information in line profiles. This paper presents such a model.

2. THE MODEL

The model assumes two uniform regions along the line of sight with velocity dispersion σ and peak optical depth τ_0. In the front and rear, the excitation temperatures are T_f and T_r, the systemic velocities are $\langle V_f\rangle$ and $\langle V_r\rangle$, each $\geq$0, and the optical depths are

$$\tau_f = \tau_0 \exp\left[-(v - \langle V_f\rangle)^2/2\sigma^2\right], \quad (1a)$$

$$\tau_r = \tau_0 \exp\left[-(v + \langle V_r\rangle)^2/2\sigma^2\right]. \quad (1b)$$

The line brightness temperature is easily obtained from the equation of radiative transfer as

$$\Delta T_B = J(T_f)[1 - e^{-\tau_f}] + J(T_r)[1 - e^{-\tau_r}]e^{-\tau_f} - J(T_b)[1 - e^{-\tau_r - \tau_f}], \quad (2)$$

where $J(T) \equiv T_0/[\exp\ (T_0/T) - 1]$ is the Planck-corrected brightness temperature, $T_b = 2.7$ K is the temperature of the cosmic background, and $T_0 \equiv h\nu/k$, where ν is the transition frequency, and h and k represent Planck's and Boltzmann's constants, respectively.

Despite their simplicity, equations (1) and (2) reproduce the two-peak profiles associated with inward motions, if $\tau_0 \gtrsim 3$, $T_r > T_f$, and $\langle V_f\rangle + \langle V_r\rangle < \sim\sigma$. The corresponding "thin" line, whose peak lies between the two thicker peaks, also follows if $\tau_0 \lesssim 1$. This combination of optical depth, inward increase in excitation temperature, and inward motion needed here to match the "infall" profiles is also needed in more detailed models (e.g., Leung & Brown 1977). However, equations (1) and (2) by themselves are too idealized and have too many parameters (six) to be useful.

To reduce the number of parameters, we replace $\langle V_f\rangle$, $\langle V_r\rangle$, T_f, and T_r in equations (1) and (2) by values characteristic of the front and rear halves of a centrally condensed, contracting cloud following power laws of density and velocity. These characteristic values should be values where $\tau_f \approx 1$ and $\tau_r \approx 1$ when $\tau_0 \gg 1$, and should be the opacity-weighted means along the line of sight when $\tau_0 < 1$. Therefore, we obtain the characteristic velocities by evaluating the attenuation-weighted means,

$$\langle V_f\rangle = \int_0^{\tau_0} d\tau_f V_f \exp(-\tau_f) \Big/ \int_0^{\tau_0} d\tau_f \exp(-\tau_f), \quad (3a)$$

$$\langle V_r\rangle = \int_0^{\tau_0} d\tau_r V_r \exp(-\tau_r) \Big/ \int_0^{\tau_0} d\tau_r \exp(-\tau_r). \quad (3b)$$

Similarly, we obtain each characteristic excitation temperature from the corresponding attenuation-weighted mean density and a two-level model of excitation.

We adopt power laws of density $n/n_{\rm max} = (r/r_{\rm min})^{-3/2}$ and infall speed $V/V_{\rm max} = (r/r_{\rm min})^{-1/2}$, the asymptotic behavior expected from a collapsing isothermal sphere (e.g., Shu 1977). The radius $r_{\rm min}$ is set in principle by departure from spherical symmetry, e.g., at the "centrifugal barrier" (Terebey, Shu, & Cassen 1984), and in practice by the observational resolution. The peak optical depths along the central line of sight from r to $r_{\rm max}$ in front and from r to $r_{\rm min}$ in the rear are

$$\tau_f = \tau_0 \frac{r^{-1/2} - r_{\rm max}^{-1/2}}{r_{\rm min}^{-1/2} - r_{\rm max}^{-1/2}}, \tag{4a}$$

$$\tau_r = \tau_0 \frac{r_{\rm min}^{-1/2} - r^{-1/2}}{r_{\rm min}^{-1/2} - r_{\rm max}^{-1/2}}. \tag{4b}$$

In obtaining equation (4), we neglect the variation of excitation temperature and partition function, which are relatively small compared with the variation of r, and we assume small velocity gradients, i.e., $V_{\rm max} \leq \sigma$. We assume that the observable spatial extent, $r_{\rm max}$, is much greater than $r_{\rm min}$, yielding

$$\frac{n}{n_{\rm max}} = \left(\frac{V}{V_{\rm max}}\right)^3 = \left(\frac{\tau_f}{\tau_0}\right)^3 = \left(1 - \frac{\tau_r}{\tau_0}\right)^3. \tag{5}$$

Then integration as in equation (3) yields

$$\frac{\langle n_f \rangle}{n_{\rm max}} = (1 - e^{-\tau_0})^{-1}\left[\frac{6}{\tau_0^3} - e^{-\tau_0}\left(1 + \frac{3}{\tau_0} + \frac{6}{\tau_0^2} + \frac{6}{\tau_0^3}\right)\right], \tag{6a}$$

$$\frac{\langle n_r \rangle}{n_{\rm max}} = (1 - e^{-\tau_0})^{-1}\left[1 - \frac{3}{\tau_0} + \frac{6}{\tau_0^2} - \frac{6}{\tau_0^3}(1 - e^{-\tau_0})\right]. \tag{6b}$$

Both ratios in equation (6) have the same optically thin limit (as $\tau_0 \rightarrow 0$), $n_{\rm thin}/n_{\rm max} = \frac{1}{4}$. Similarly,

$$\frac{\langle V_f \rangle}{V_{\rm max}} = \frac{1 - (1 + \tau_0)e^{-\tau_0}}{\tau_0(1 - e^{-\tau_0})}, \tag{7a}$$

$$\frac{\langle V_r \rangle}{V_{\rm max}} = \frac{\tau_0 - (1 - e^{-\tau_0})}{\tau_0(1 - e^{-\tau_0})}, \tag{7b}$$

with a common optically thin limit $V_{\rm thin}/V_{\rm max} = \frac{1}{2}$. We adopt as inward speed parameter $V_{\rm in} \equiv V_{\rm thin}$. Thus, two lines observed from the same position with the same resolution (which sets $r_{\rm min}$) should have the same value of $V_{\rm in}$. Clouds with progressively greater values of $V_{\rm max}$, as expected for progressively more advanced stages of infall, should have progressively greater values of $V_{\rm in}$.

To obtain excitation temperatures T_f and T_r, we assume that $n_{\rm thin}$, the characteristic density when $\tau_0 \rightarrow 0$, equals $n_{\rm cr}$, the critical density in a two-level excitation model (e.g., Rank, Townes, & Welch 1971). This assumption is plausible for lines as in § 3, which are detectable without photon trapping: their intensity and shape at the map edge are consistent with $\tau < \sim 1$. Then

$$\frac{T_f}{T_k} = \frac{T_b + (4T_0/\beta)\langle n_f \rangle/n_{\rm max}}{T_k + (4T_0/\beta)\langle n_f \rangle/n_{\rm max}}, \tag{8a}$$

$$\frac{T_r}{T_k} = \frac{T_b + (4T_0/\beta)\langle n_r \rangle/n_{\rm max}}{T_k + (4T_0/\beta)\langle n_r \rangle/n_{\rm max}}, \tag{8b}$$

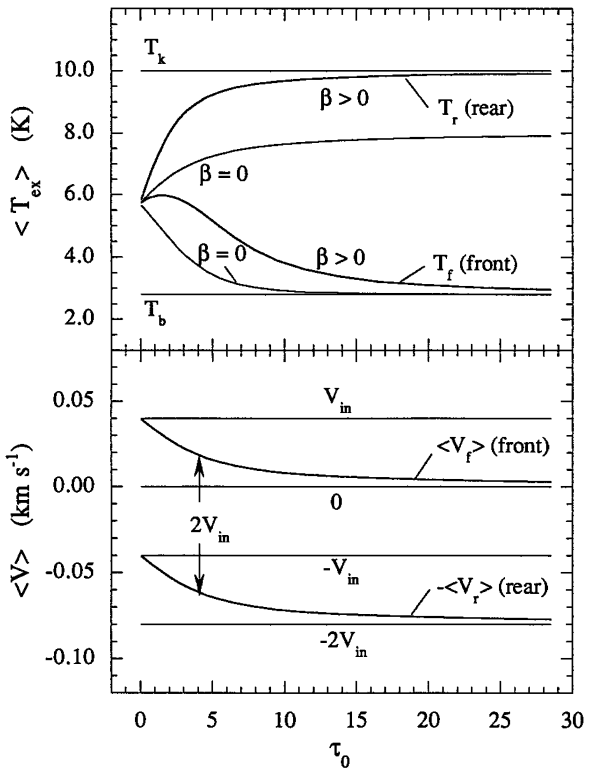

FIG. 1.—Characteristic excitation temperature (*top*) and velocity (*bottom*) vs. peak optical depth τ_0 in the front and rear halves of a spherically symmetric cloud with density $n/n_{\rm max} = (r/r_{\rm min})^{-3/2}$ and infall speed $V/V_{\rm max} = (r/r_{\rm min})^{-1/2}$. The excitation temperature is shown with ($\beta > 0$) and without ($\beta = 0$) the contribution from photon trapping. The difference in characteristic velocity between front and rear maintains a constant value $2V_{\rm in}$, independent of τ_0. As τ_0 increases, $\langle T_{\rm ex} \rangle$ and $\langle V \rangle$ become hot and fast in the rear, and slow and cold in the front.

with T_k the kinetic temperature and $\beta = [1 - \exp(-\tau_0)]/\tau_0$ the escape probability (e.g., Shu 1991).

The front and rear excitation temperatures T_f and T_r move apart with increasing optical depth τ_0, as shown in Figure 1 (*top*) based on equations (6) and (8). The curves are shown with and without photon trapping. In the optically thin limit, $T_f = T_r$. As τ_0 increases, the surface of unit optical depth moves forward in each half of the cloud, so T_f decreases toward T_b, but T_r increases toward T_k. This effect is quantitatively more significant than photon trapping, which heats both T_f and T_r.

The front and rear infall speeds $\langle V_r \rangle$ and $\langle V_f \rangle$ each shift to the blue with increasing optical depth τ_0, as shown in Figure 1 (*bottom*) based on equation (7). In the optically thin limit, $\langle V_f \rangle = \langle V_r \rangle = V_{\rm in}$. As τ_0 increases and the surface of unit optical depth moves forward in each half of the cloud, $\langle V_f \rangle$ approaches 0 and $\langle V_r \rangle$ approaches $2V_{\rm in}$, maintaining $V_{\rm in} = (\langle V_f \rangle + \langle V_r \rangle)/2$ for all values of τ_0.

Equations (6) and (7) specify T_f, T_r, $\langle V_f \rangle$, and $\langle V_r \rangle$ in equations (1) and (2), and reduce the number of independent adjustable parameters from 6 to 4: τ_0, T_k, $V_{\rm in}$; $\sigma_{\rm NT} \equiv (\sigma^2 - kT_k/m_{\rm obs})^{1/2}$, with $m_{\rm obs}$ the molecular mass of the observed line emitter. Inward-increasing density and velocity laws other than those assumed here give dependence of $\langle T_{\rm ex} \rangle$ and $\langle V \rangle$ on τ_0 similar to that in Figure 1. Analytic relations as in equations (7) and (8) follow if $n \sim r^{-p}$, $V \sim r^{-q}$, and if $p/(p-1)$ and $q/(p-1)$ are integers.

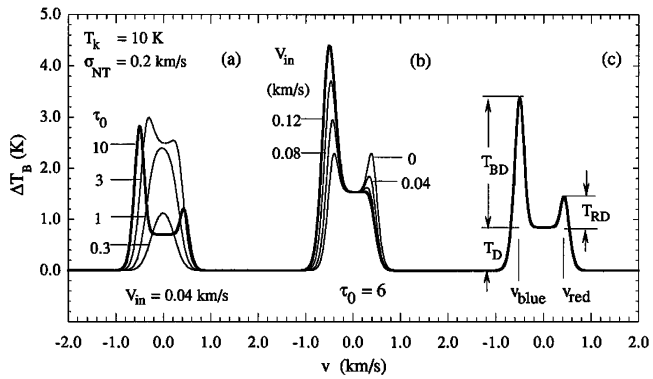

FIG. 2.—Model line profiles showing variation (*a*) with increasing peak optical depth τ_0 and (*b*) with increasing infall speed V_{in}. For "slow" infall ($V_{in} \ll \sigma$), as optical depth increases, the line brightens until it develops a self-absorption dip between a brighter blue peak and a fainter red peak. As V_{in} increases, the degree of asymmetry increases, from two equally bright peaks to a blue peak brighter than the red peak, to a blue peak and a red shoulder. The line parameters T_D, T_{BD}, T_{RD}, and $v_{red} - v_{blue}$ for use with eq. (9) for V_{in} are defined in (*c*).

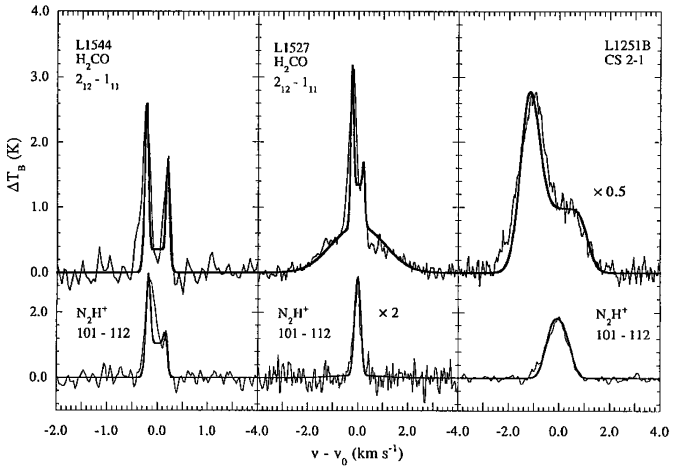

FIG. 3.—Observed and model line profiles in L1544, L1527, and L1251B. Model parameters for the upper H_2CO and CS (and lower N_2H^+) lines are, respectively, τ_0 = 15, 7.0, and 4.5 (7.0, 0.40, 0.55); σ_{NT} = 0.06, 0.09, and 0.50 (0.06, 0.09, and 0.28) km s^{-1}; T_k = 12, 11, and 12 (10, 11, and 12) K; and V_{in} = 0.006, 0.025, and 0.35 (0.02, 0.025, and 0.20) km s^{-1}. For L1527, the outflow parameters are $\tau_{0,out}$ = 0.3 (0.017) and σ_{out} = 1.0 (1.0) km s^{-1}. The model fits the line profiles well, and each optically thinner line peaks up to the red of the optically thicker peak, indicating self-absorption in a contracting cloud, rather than two velocity components.

Exploring parameter space indicates that the line shape is determined mainly by τ_0 and V_{in}/σ_{NT}, in accord with the conclusion of Leung & Brown (1977) for a wide variety of infall systems. Figure 2*a* shows profiles as τ_0 increases from thin to thick values, while the infall speed V_{in} is fixed at a relatively small fraction ($\frac{1}{5}$) of the nonthermal velocity dispersion σ_{NT}. As τ_0 increases, the line becomes more intense, until it develops a self-absorption dip. Then the intensities of the dip and the red peak decrease, while the intensity of the blue peak increases. This progression of profile asymmetry with optical depth is similar to that seen in more detailed models of infall and radiative transfer cited earlier. Figure 2*b* shows profiles as V_{in} increases from 0 to 0.6 σ_{NT}, with fixed $\tau_0 = 6$. The two peaks start with equal intensity, then the blue peak increases while the red peak decreases. At larger values of V_{in}, the red peak disappears, so that the profile has a single peak in the blue and a red shoulder.

The progressions of profiles in Figures 2*a* and 2*b* can be understood in terms of a "rear profile" arising if the front half of the cloud were absent, and a "front profile" arising if the rear half were absent. For $\tau_0 \ll 1$, these two profiles are identical in intensity and in their Gaussian shape, but have a shift $2V_{in}$ in their line centers. As τ_0 exceeds 1, each profile gets brighter and starts to saturate, approaching higher intensities in the rear than in the front, as expected from Figure 1. Also, as τ_0 increases, the cool front gas absorbs an increasing portion of the warm rear emission. For $V_{in}/\sigma < 1$, this absorption forms two peaks and a dip in the combined profile, centered on $\langle V_f \rangle$. These peaks occur approximately at the two velocities where $\tau_f = 1$. These two velocities are redder than those where $\tau_r = 1$, so the blue peak is brighter than the red. If τ_0 and V_{in}/σ are each sufficiently large, the red peak disappears into a red shoulder, because then, at the redder velocity where $\tau_f = 1$, the front emission exceeds the attenuated rear emission.

This analysis can be quantified to estimate the infall speed for a two-peak line solely in terms of observable line parameters. Our model profiles indicate that the difference $v_{red} - v_{blue}$ between the velocities of the red and blue peaks approximately equals the difference between the velocities where $\tau_f = 1$, and we assume this is true exactly. Assuming further that $V_{in} \ll \sigma(2 \ln \tau_0)^{1/2}$, we obtain from equations (1) and (2) the general result, independent of any distributions of V or n,

$$V_{in} \approx \frac{\sigma^2}{v_{red} - v_{blue}} \ln\left(\frac{1 + eT_{BD}/T_D}{1 + eT_{RD}/T_D}\right), \qquad (9)$$

where, as in Figure 2*c*, T_D is the brightness temperature of the dip (assumed optically thick), T_{BD} is the height of the blue peak above the dip, and T_{RD} is the height of the red peak above the dip. The velocity dispersion σ can be obtained from the FWHM of a suitable optically thin line. Tests of equation (9) were made by computing profiles with $\tau_0 = 5$ and 10, $T_k = 10$ K, $\sigma_{NT} = 0.07$ km s^{-1}, and V_{in} ranging from 0 to ~2 σ_{NT}, where the red peak disappears. In these tests, the V_{in} based on equation (9) departs from the V_{in} assumed to calculate the profile by less than ~20%.

3. COMPARISON WITH OBSERVATIONS

The model matches observed profiles with widely different shapes, as shown in Figure 3 for thicker lines (H_2CO 2_{12}–1_{11} and CS 2–1) and thinner lines (N_2H^+ JF_1F = 101–012). In L1251B, the CS line is used because it demonstrates a red shoulder more clearly than does the H_2CO line. The peak of the thinner line lies between the two peaks of the thicker line in L1544 and L1527, and between the blue peak and the red shoulder in L1251B—consistent with contraction and self-absorption, and inconsistent with two independent clouds along the line of sight. In Figure 3 (*legend*), the derived values of σ_{NT} and V_{in}/σ_{NT} differ from the "thick" to the "thin" fit in two of six cases; where a choice is needed, we favor the better-constrained "thick" values.

In L1544, the observed 2 mm line of H_2CO (Tafalla et al. 1996) is narrow, with a deep dip and no wings. L1544 has no associated *IRAS* source, no known CO outflow, and weak submillimeter emission (Ward-Thompson et al. 1994). The model profile requires high optical depth, $\tau_0 = 15$, for the deep

dip, narrow velocity dispersion, $\sigma_{NT} = 0.06$ km s^{-1}, for the small separation of peaks, and extremely "slow" infall, $V_{in}/\sigma_{NT} = 0.1$, for the slight asymmetry of peak intensities. The model fits the observed peak and dip intensities, with slightly narrower peaks than observed. The speed $V_{in} = 0.006$ km s^{-1} has 1 σ uncertainty 0.002 km s^{-1} based on the propagation of errors in equation (9).

In L1527, the observed 2 mm line of H_2CO is broader than in L1544, and has a strong blue peak and a weak red peak. The embedded class 0 protostar is relatively isolated and has weak outflow wings. The ratio of peak intensities, 2.2, is difficult to match with a model based on spherically symmetric inside-out collapse (Myers et al. 1995). The present model fits well. The velocity dispersion and infall speed are each greater than in L1544, by factors of 1.5 and 4.2, respectively. The weak outflow wings are fitted by adding a central outflow zone with peak optical depth $\tau_{0,\,out}$ and velocity dispersion σ_{out}. Then the infall parameters change only slightly from the no-outflow case.

In L1251B, the observed 3 mm line of CS 2–1 (Mardones et al. 1996) is much broader than in L1527, and it has a blue peak with a red shoulder. L1251B has a red *IRAS* source with luminosity 6 $L_\odot$, a weak outflow (Sato & Fukui 1989), and an associated group of at least five near-infrared sources within ~0.02 pc (Hodapp 1994). The model fit requires a velocity dispersion 0.5 km s^{-1}, ~5 times greater than in L1527, "fast" infall, with $V_{in}/\sigma_{NT} = 0.7$ and no outflow.

4. PHYSICAL IMPLICATIONS AND DISCUSSION

The parameter values in Figure 3 indicate motions consistent with gravitational infall. For the radius over which infall asymmetry is seen, we adopt $r_{in} = 0.027$, 0.014, and 0.029 pc in L1544, L1527, and L1251B, respectively, each based on mapping observations and uncertain by a factor of ~1.5 (Mardones et al. 1996; Myers et al. 1995; Tafalla et al. 1996). We estimate the "kinematic" mass infall rate dM/dt from $4\pi r_{in}^2 m n_{cr} V_{in}$, yielding, respectively, 1.9, 2.1, and 40×10^{-6} $M_\odot$ yr^{-1}, each with observational uncertainty of a factor ~2, and we estimate the "gravitational" rate from $a^3\ G^{-1}$ (Shu 1977), yielding 2.5, 2.5, and 37×10^{-6} $M_\odot$ yr^{-1}, each uncertain by a factor ~1.5. Here a is the velocity dispersion of the molecule of mean mass m, $a^2 = kT/m + \sigma_{NT}^2$. The agreement of these two rates in each source indicates that the derived inward motions are consistent with gravitational infall. Further, this consistency holds for sources at different stages of star formation, with different physical conditions: the velocity dispersion is primarily thermal in L1544 and L1527, but primarily nonthermal in L1251B. These results should not be considered definitive unless they are confirmed by more detailed observations, but they already indicate a promising way to derive and apply infall parameters from line profiles.

The two-peak and red-shoulder profiles predicted by this idealized model resemble those of more detailed codes. Although the red-shoulder profiles in Figure 2*b* and 3*c* are not well known as indicators of infall, they are predicted in the detailed numerical models of Dickel & Auer (1994). These authors compute profiles for a density law $n \sim r^{-3/2}$ and a velocity law $V \sim r^{-1/2}$ as in this paper, and also for "inside-out" collapse (V decreasing to zero more rapidly than $\sim r^{-1/2}$). They find that the $V \sim r^{-1/2}$ model gives a pronounced red shoulder (their Fig. 5, *top right*), while the inside-out model gives a profile with slight asymmetry but no shoulder (their Fig. 5, *bottom right*).

The present model is limited because it treats the continuously varying density and velocity fields as a pair of densities and velocities, set by the optical depth at line center. Thus, the model cannot predict optically thin "infall wings" from gas near the cloud center (e.g., Zhou et al. 1993). This simplified structure also accounts for the narrower widths, steeper slopes, and flatter dips of the profile features in the model than in the observations. The model also applies to relatively small offsets from cloud center compared with the cloud radius; this limits the study of how profiles vary with changes in resolution and cloud position.

Despite these and other limitations, the model is evidently able to fit a variety of profiles from candidate infall regions, including those with a large ratio of blue and red peak intensities. The model provides a simple way to quantify characteristic infall speeds. The model spectra in Figure 3 are not unique with respect to parameter variation or to changes in velocity and density laws, and it will be important to quantify these variations. Nonetheless, it seems unlikely that the derived order of infall speeds from L1544 to L1527 to L1251B will depend on such factors.

D. M. thanks the Carnegie Foundation, and M. T., J. P. W., and D. J. W. thank the Harvard-Smithsonian Center for Astrophysics for fellowship support. This research was supported by NASA Origins of Solar Systems Program, grant NAGW-3401.

REFERENCES

Bernes, C. 1979, A&A, 73, 67
Choi, M., Evans, N. J., Gregersen, E. M., & Yang, Y. 1995, ApJ, 448, 742
Dickel, H. R., & Auer, L. H. 1994, ApJ, 437, 222
Gregerson, E., Evans, N. J., Zhou, S., & Choi, M. 1996, in preparation
Hodapp, K.-W. 1994, ApJS, 94, 615
Leung, C. M. 1978, ApJ, 225, 427
Leung, C. M., & Brown, R. L. 1977, ApJ, 214, L73
Mardones, D., Bachiller, R., Myers, P. C., & Tafalla, M. 1996, in preparation
Mardones, D. M., Myers, P. C., Caselli, P., & Tafalla, M. 1994, in ASP Conf. Ser. 65, Clouds, Cores, and Low-Mass Stars, ed. D. Clemens & R. Barvainis (San Francisco: ASP), 192
Myers, P. C., Bachiller, R., Caselli, P., Fuller, G. A., Mardones, D., Tafalla, M., & Wilner, D. J. 1995, ApJ, 449, L65
Rank, D. M., Townes, C. H., & Welch, W. J. 1971, Science, 174, 1083
Sato, F., & Fukui, Y. 1989, ApJ, 343, 773
Shu, F. H. 1977, ApJ, 214, 488
———. 1991, in The Physics of Astrophysics, Vol. 1, Radiation (Mill Valley: University Science Books)
Tafalla, M., Bachiller, R., Mardones, D., & Myers, P. C. 1996, in preparation
Terebey, S., Shu, F. H., & Cassen, P. 1984, ApJ, 286, 529
Walker, C. K., Lada, C. J., Young, E. T., Maloney, P. R., & Wilking, B. A. 1986, ApJ, 449, L65
Walker, C. K., Narayanan, G., & Boss, A. P. 1994, ApJ, 431, 767
Wang, Y., Evans, N. J., Zhou, S., & Clemens, D. P. 1995, ApJ, 454, 217
Ward-Thompson, D., Scott, P. F., Hills, R. E., & André, P. 1994, MNRAS, 268, 276
Zhou, S., Evans, N. J., Kompe, C., & Walmsley, C. M. 1993, ApJ, 404, 232
Zhou, S., Evans, N. J., Wang, Y., Peng, R., & Lo, K. Y. 1994, ApJ, 433, 131